Regular article

UV, five wavelengths fusion and electrochemical fingerprints combined with antioxidant activity for quality control of antiviral mixture

Kaining Zhou, Zini Tang, Guoxiang Sun*, Ping Guo*, Lili Lan*

College of Pharmacy, Shenyang Pharmaceutical University, Shenyang 110016, China

Abstract

Aiming to ensure the consistency of quality control of Traditional Chinese Medicines (TCMs), a combination method of high-performance liquid chromatography (HPLC), ultraviolet (UV), electrochemical (EC) was developed in this study to comprehensively evaluate the quality of Antiviral Mixture (AM), and Comprehensive Linear Quantification Fingerprint Method (CLQFM) was used to process the data. Quantitative analysis of three active substances in TCM was conducted. A five-wavelength fusion fingerprint (FWFF) was developed, using second-order derivatives of UV spectral data to differentiate sample levels effectively. The combination of HPLC and UV spectrophotometry, along with electrochemical fingerprinting (ECFP), successfully evaluated total active substances. Ultimately, a multidimensional profiling analytical system for TCM was developed.

Keywords: TCM; antiviral mixture; five-wavelength fusion fingerprint (FWFF); Comprehensive Linear Quantification Fingerprint Method (CLQFM); quantization fingerprint; antioxidant activity profilling

1 Introduction

Traditional Chinese Medicine (TCM) is medicine developed on the basis of effective Chinese Medicine Prescriptions to meet the needs of diagnosis and treatment. It is mostly compound preparation with complex components from wide sources. However, there is little research on TCM quality control, so it is necessary to establish a novel control method. Antiviral Mixture (AM) has good effects of clearing heat and detoxifying, calming the liver and resolving blood stasis, and resisting virus, and is used to treat viral skin diseases such as flat warts and herpes zoster caused by heat toxicity. AM is formulated from ten kinds of herbs, including Gleditsiae Spina, Lonicerae Japonicae Flos, Scutellariae Radix, Carthami Flos, Isatidis Radix, Lonicerae Japonicae Caulis, Ostreae Concha, Margaritifera Concha, Haematitum, and Magnetitum. Its chemical composition will be affected by a range of factors, such as cultivation area, prevailing climate conditions, and storage environment. Furthermore, there are potential problems in

* Author to whom correspondence should be addressed. Address: School of Traditional Chinese Materia Medica, Shenyang Pharmaceutical University, 103 Wenhua Rd., Shenyang 110016, China; Tel.: +86-13940272571 (Guoxiang Sun); E-mail: gxswmwys@163.com (Guoxiang Sun), lanlily1314@163.com (Lili Lan), guoping20023@163.com (Ping Guo).

Received: 2024-03-07 Accepted: 2024-05-02

the production process, such as contamination, presence of heavy metals, pesticide residues and the possibility of adulteration. Therefore, it is necessary to put forward a novel compound TCM [1]. In order to ensure the consistent quality of TCM, the comprehensive multidimensional fingerprint, a comprehensive analytical technique, was employed. It captures various aspects of the chemical constituents presented in the herbs and effectively controls their overall chemicals. By utilizing them to assess the types and quantities of chemicals in herbal medicines, we can not only identify the authenticity but also control the consistency of TCM quality [2].

Currently, high performance liquid chromatography (HPLC) provides rich information about the composition of TCM and is widely used for quality control [3-7]. Ultraviolet (UV) spectroscopy is also widely used nowadays because it can meet the requirements of inclusive analysis [8], It uses flow injection analysis (FIA) to evaluate the overall quality of substances containing unsaturated bonds and conjugated groups qualitatively and quantitatively [9], an useful complement for HPLC. What is more, the full UV wavelength spectrum can be quickly obtained by using DAD detector.

Professor Guoxiang Sun [10] proposed spectral quantum fingerprinting [11], which can transform the UV wavelength spectrum, Fourier Transform infrared spectrum and THz spectrum of TCM into easily profiled one by Systematically Quantified Fingerprint Method [12-14]. Among them, the UV quantum fingerprint can is used to evaluate the grade of the samples, electrochemistry is used for identification, quantification and quality evaluation of TCM [15], and the electrochemical profiles of the B-Z oscillation system is used to explore the relationship between various ECFP fingerprints.

In this study, the antioxidant profiling was applied in HPLC fingerprint and UV quantum profiling by gray correlation. Finally, the comprehensive HPLC and UV combined with ECFP were developed as a novel method to evaluate the quality consistency of TCM. The flow chart of the study was shown in Fig. 1.

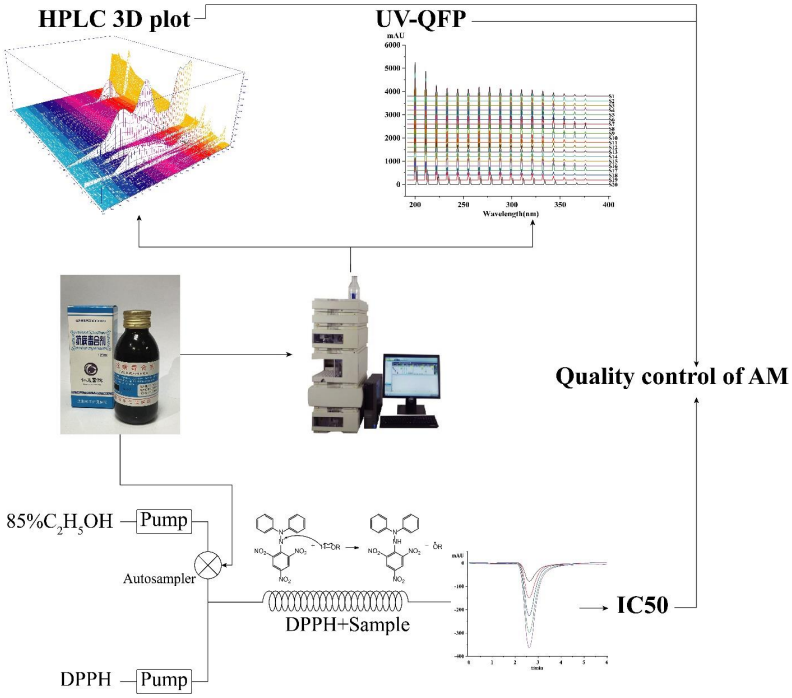

Fig. 1 Flow chart of the study

2 Theory

2.1 Theory of CLQFM

The Comprehensive Linear Quantitative Fingerprint Method (CLQFM) provides three important parameters: comprehensive linear qualitative similarity $\boldsymbol{S}_L$, comprehensive linear quantitative similarity $\boldsymbol{P}_L$ and Fingerprint coefficient of variation $\boldsymbol{\alpha}$.

The reference fingerprint vector $\vec{X} = (x_1, x_2, ..., x_i)$ is used as the independent variable, and the sample fingerprint vector $\vec{Y} = (y_1, y_2, ..., y_i)$ as the dependent variable, where x_i and y_i represent the peak areas of the i-th component of the reference fingerprint and sample fingerprint vectors, respectively. The linear formula $\vec{X} = a + b\vec{Y}$ can be used to solve the sample fingerprints, including several reference fingerprints. The correlation coefficient (r) of the linear equation is defined as linear qualitative similarity [16]. The reference fingerprint vector is $\overrightarrow{XS} = (1, 1, \ldots, 1)$, and the sample fingerprint vector is $\overrightarrow{YS} = (x_1/y_1, x_2/y_2, \ldots, x_n/y_n)$. To eliminate the influence of large peaks on r in the fingerprint, S'_F (cosine value of the angle between two vectors) is used for correction. The linear qualitative similarity $\boldsymbol{S}_L$ is obtained from averaging the combination of r and S'_F, as shown in Equation (1), which can fully reflect the characteristics of the number and distribution of chemical fingerprint components in TCM. The slope b in the linear equation $\vec{X} = a + b\vec{Y}$ can be calculated, in which, b is defined as the linear quantitative similarity, which can quantitatively compare $\vec{X}$ and $\vec{Y}$. In order to eliminate the error caused by different x_i/y_i cross compensation, the ratio of the quality m_R of the reference fingerprint to the quality m_n of the sample is used for correction in the calculation. Therefore, b is defined as the linear quantitative similarity, which can quantitatively compare $\vec{X}$ and $\vec{Y}$. Considering that different fingerprint peak areas compensate each other when they are added, r correction should be performed to obtain the corrected linear quantitative similarity rb. R is the macro content similarity, the ratio of the total integral area of the sample fingerprint to the total integral area of the reference fingerprint, as shown in Equation (2). After S'_F correction, the corrected macro content similarity RS'_F is obtained. The comprehensive linear quantitative similarity S'_F is obtained by combining S'_F with linear average and geometric average, as shown in Equation (3), which can fully measure the similarity of the overall content of the chemical fingerprint.

Fingerprint variation coefficient $\boldsymbol{\alpha}$ is obtained from Equation (4) by b and R, which can monitor the accuracy of the linear fingerprint model. At the same time, considering the three indicators $\boldsymbol{S}_L$, $\boldsymbol{P}_L$ and $\boldsymbol{\alpha}$, the quality level of TCM is classified as shown in Table 1 [17].

$$\boldsymbol{S}_L = \sqrt{\frac{1}{2}(r + S'_F)\sqrt{rS'_F}} = \sqrt{\frac{1}{2}\left(\frac{\sum_{i=1}^{n}(x_i-\overline{x_i})(y_i-\overline{y_i})}{\sqrt{\sum_{i=1}^{n}(x_i-\overline{x_i})^2}\sqrt{\sum_{i=1}^{n}(y_i-\overline{y_i})^2}} + \frac{\sum_{i=1}^{n}\frac{x_i}{y_i}}{\sqrt{n\sum_{i=1}^{n}(\frac{x_i}{y_i})^2}}\right)\sqrt{\frac{\sum_{i=1}^{n}(x_i-\overline{x_i})(y_i-\overline{y_i})}{\sqrt{\sum_{i=1}^{n}(x_i-\overline{x_i})^2}\sqrt{\sum_{i=1}^{n}(y_i-\overline{y_i})^2}} \times \frac{\sum_{i=1}^{n}\frac{x_i}{y_i}}{\sqrt{n\sum_{i=1}^{n}(\frac{x_i}{y_i})^2}}}} \quad (1)$$

$$R = \frac{\overline{x}}{\overline{y}} = \frac{a}{\overline{y}} + b = \frac{a}{\overline{y}} + \frac{n\sum_{i=1}^{n}x_iy_i - \sum_{i=1}^{n}x_i\sum_{i=1}^{n}y_i}{n\sum_{i=1}^{n}y_i{}^2 - \left(\sum_{i=1}^{n}y_i\right)^2} \times 100\% \times \frac{m_R}{m_n} \quad (2)$$

$$\boldsymbol{P}_L = \sqrt{\frac{1}{2}(rb + RS'_F)\sqrt{rbRS'_F}} \quad (3)$$

$$\alpha = \left|\frac{R}{b} - 1\right| \quad (4)$$

2.2 Mechanism of the B-Z oscillating system

The B-Z oscillatory system is a dynamic system in which malonic acid ($CH_2(COOH)_2$) is oxidated by potassium bromate ($KBrO_3$) in Sulfuric acid (H_2SO_4) using cerium ions as a catalyst for the mechanism of the redox reaction. The reaction was homogenized by stirring at constant temperature, while the curves of [Br^-] and [Ce^{4+}]/[Ce^{3+}] with time were measured by saturated calomel electrode and platinum electrode, respectively, and converted into potential-time curves by electrochemical workstation, and finally the sample grade was evaluated by CLQFM method.

The FKN mechanism [18] successfully explains the B-Z oscillatory reaction, including two main parts, namely the induction process (A,B) and the oscillatory process (C,D,E), as shown in Fig. 2A. When the potassium bromate is added, the process A and B occur first, bromide ions are continuously generated, and a critical concentration of [Br^-] happens in the process. When [Br^-] becomes higher than $[Br^-]_{crit}$, the oscillatory process is initiated, and 6-8 consumption of bromide ions occurs first. When [Br^-] becomes less than $[Br^-]_{crit}$, process D is initiated and Br^- is regenerated, and the process E occurs. The continuous circulation of these three processes shows that the b-z oscillation reaction is going on. All substances except malonic acid undergo the cycle of "depletion-regeneration" in the oscillatory reaction, and their concentration constantly changes with time, which is reflected in the fluctuation curve of the potential-time diagram. At the same time, as a dissipative substance, malonic acid will gradually reduce without replenishment, which will slow down the reaction, and eventually reach equilibrium and terminate. It is shown in the E-T diagram that the fluctuation of the curve is gradually stabilized. After the sample to be tested is added, the sample components will react with potassium bromate and interfere with the original system, so that the reaction can reach equilibrium faster. The antioxidant capacity of the samples affects the degree of inhibition, which leads to the different reaction lifetimes.

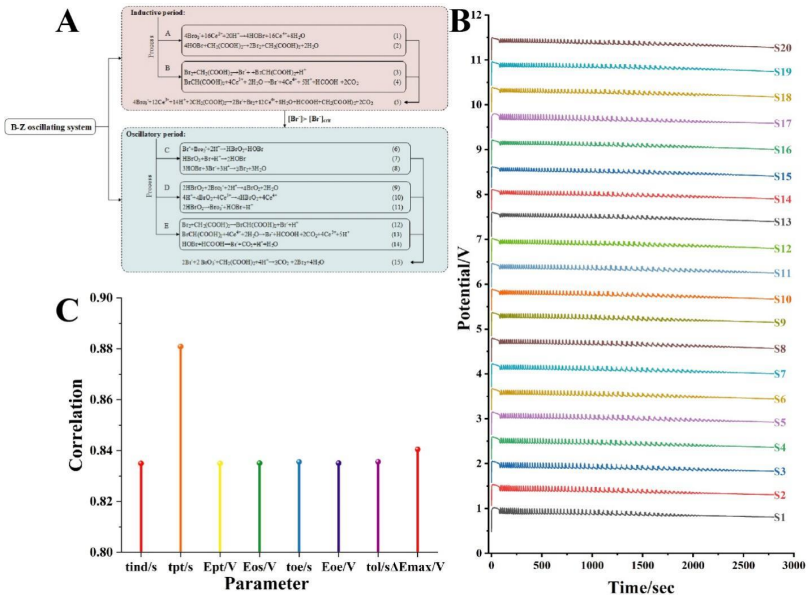

Fig. 2 Electrochemical schematic diagrams (A), E-T curves of electrochemical samples (B) and grey correlation of electrochemical parameters with *E* values (C)

3 Materials and methods

3.1 Samples and chemical reagents

20 batches of samples numbered S1-S20 were produced in the preparation room of Shenyang Heping RenSheng Hospital.

Standard reference substances, namely chlorogenic acid (CA) and isochlorogenic acid-A (IA), were purchased from Chengdu Aifa Biotechnology Co., Ltd., Baicalin (Bai) was purchased from National Institutes for Food and Drug Control, HPLC grade acetonitrile, methanol, and isopropanol were obtained from Shandong Yuwang Industry Co., Ltd., phosphoric acid was supplied by Tianjin kemeo Chemical Reagent Co., Ltd., and Heptane sulfonate sodium was supplied by China US chromatography products factory, Yucheng, Shandong Province, China. Deionized water was used in the experiments and other chemicals were analytically pure. 98% concentrated sulfuric acid was provided by Lianlong Bohua (Tianjin) Pharmaceutical Chemical Co., Ltd; Potassium bromate was provided by Tianjin Kemio Chemical Reagent Co., Ltd; Malonic acid and potassium chloride were provided by Tianjin Damao Chemical Reagent Factory; Ceric ammonium sulfate were provided by Tianjin Bodi Chemical Co., Ltd. They are all analytically pure.

3.2 Sample and standard solution preparation

3.2.1 Test solution preparation

For HPLC, UV and EC analysis, the sample solution was filtered with a 0.45 μm filter membrane, and the continuous filtrate was obtained as the test solution. For antioxidant activity test, AM samples were filtered with a 0.45 μm filter membrane, and diluted five times with deionized water as the test solution.

3.2.2 Standard solution preparation

Three chemicals were precisely weighed and dissolved in methanol to provide standard solutions of 0.13 mg/mL CA, 0.05 mg/mL IA and 0.46 mg/mL Bai. All samples and standard solutions were stored at 4 ℃ before analysis.

3.3 Instruments and experimental conditions

3.3.1 HPLC analysis

HPLC experiments were performed with an Agilent 1100 HPLC series instrument (Agilent Technologies, USA) consisting of an autosampler, an in-line degasser, a low-pressure hybrid quaternary pump and a diode array detector (DAD). System control and data acquisition were performed using an Agilent Chemstation (Agilent USA). The COSMOSIL C-18 column (250 mm × 4.6 mm, 5 μm) with the temperature of 35 ℃ was used.

The mobile phase was 5 mmol/L sodium 1-heptane sulfonate phosphoric acid (0.2% (V/V) in water (A) and acetonitrile methanol (9:1, V/V) (B) and the flow rate was 1.0 mL/min. The gradient elution sequence was as follows: 94-79% A (0-10 min); 79-65% A (10-30 min); 65-45% A (30-55 min); 45-18% A (55-65 min); 18-15% A (65-70 min); 15-15% A (70-75 min); 15-94% A (75-80 min). The injection volume was 5.0 μL. The data at wavelengths of 220 nm, 238 nm, 254 nm, 278 nm and 326 nm were recorded, of which 238 nm was the quantitative detection wavelength.

3.3.2 UV spectrum analysis

UV spectra were recorded at 1 nm intervals in range of 190-400 nm and chromatograms of samples were detected at 220 nm by using the Agilent 1100 HPLC system mentioned in Section 3.3.1 in which the chromatographic column was replaced by a

polyetheretherketone (PEEK) tube (5000 mm × 0.12 mm). The mobile phase, acetonitrile/methanol (9:1, v/v), entered into DAD. 5 μL of sample solution was injected with a flow rate of 0.5 mL/min.

3.3.3 Preparation of EC oscillation system solution

The electrochemical oscillation system was investigated using a CHI 700E series double potentiostat. The working electrode employed in the study was a platinum electrode (type CHI 115, Shanghai Chenhua Instrument Co., Ltd.). As for the reference electrode, a double liquid connection calomel electrode was utilized (type 217, Tianjin Labia Technology Development Co., Ltd.). Experimental conditions were maintained using an HH-501 super constant temperature water bath pot, and stirring was facilitated by an 85-2A digital display constant temperature magnetic stirrer from Jiangsu Jintan Jincheng Guosheng Experimental Instrument Factory.

In a custom-made 40 mL reactor, 12 mL of 2.0 mol/L sulfuric acid solution (H_2SO_4) was mixed with 6 mL of 0.3 mol/L propane diacid solution ($CH_2(COOH)_2$) and 3 mL of 0.04 mol/L ceric ammonium sulfate solution (prepared using a 0.2 mol/L H_2SO_4 solution). The mixture was stirred at 400 r/min for 5 min at 37 ℃. Subsequently, 3 mL of 0.3 mol/L potassium bromate ($KBrO_3$) solution was added to make the total volume reach 24 mL, thus forming the blank Belousov-Zhabotinsky (B-Z) oscillating system. The sample assay was carried out by adding 0.5 mL of AM to the blank system.

3.3.4 Online in vitro antioxidant analysis

Mobile phase A ethanol-water (A) (85:15, V/V) as carrier at a flow rate of 0.4 mL/min and mobile phase B as 0.066 mg/mL of 1,1-Diphenyl-2-picrylhydrazyl (DPPH) methanol solution at a flow rate of 0.3 mL/min were mixed at a tee and passed into a center-contained PEEK tube (5000 mm × 0.18 mm). Analysis was carried out using flow injection analysis, where the sample and DPPH solution reacted in a hollow peek tube and finally passed through a DAD detector to detect the absorbance of the mixture at 517 nm. The reaction of the sample with DPPH consumes the DPPH and reduces the absorbance of the mixture solution, which results in a negative peak in the signal. The larger the negative peak area, the higher the clearance.

At the junction, the antioxidant reacts with DPPH to reduce the concentration of DPPH, thus producing an inverted peak at the stable baseline. The area of the inverted peak is directly proportional to the antioxidant capacity of the antioxidant, but it can not be quantified as a specific value. Therefore, in this study, equations (5)-(7) were used to calculate the *E*-value to express the antioxidant activity, which means how much ascorbic acid (ACA) is equivalent to 1 μL of compound. The larger the *E*-value, the stronger the antioxidant capacity.

$$y_s=a_s x+b_s \quad (5)$$

(x is the sample injection volume, and y_s is the sample peak area.)

$$y_A=a_A x+b_A \quad (6)$$

(x is the volume of the ACA injection, and y_A is the ACA's peak area.).

$$E=\frac{a_s+b_s}{a_A+b_A}\times m_A \quad (7)$$

(m_A is the mass of ACA).

3.4 Data analysis

Chromatographic fingerprints were evaluated using an in-house developed software named Digitized Evaluation System for Super-Information Characteristics of TCM Spectrum Quantum Profiling Consistency Digitized Evaluation System 4.0 (Software certificated NO. 7037415 China), second-order derivative processing of UV spectral data was performed using the Unscrambler X10.4, Origin Pro

2021 was used for statistical analysis and graphing, and A GMM Using EM Algorithm to Estimate Parameters was developed using the PyCharm community edition in the Python 3.8.1 environment.

4 Results and discussion

4.1 HPLC fingerprint analysis

4.1.1 Methodology validation

The feasibility of five-wavelength fusion fingerprint (FWFF) was verified by testing the precision, reproducibility and stability of the sample solution (S13). Precision was calculated by sequentially injecting the same S13 solution six times. Repeatability was tested by analyzing six independent S13 solutions separately. Stability of the samples was studied by injecting the solutions 6 times within 24 h under the same experimental conditions. Finally, reliability was calculated by calculating the RSD value of the $\boldsymbol{P}_L$% of the samples. The RSDs of precision, reproducibility and stability were 0.28%, 0.43% and 0.66%, respectively, indicating that the method can be used for the determination of HPLC profiles of the samples.

AM with 10 herbs contains a variety of active substances with antioxidant, antibacterial and antitumor properties. Here, three pharmacophoric substances (CA, IA and Bai) were identified and quantified by comparing the retention time and 3D plot (Fig. 3E) of the samples and the control solution. The retention time of CA, IA and Bai at 238 nm was 10.3, 17.3 and 23.2 min for the 6th, 9th and 16th peaks, respectively. The structures and peak positions are shown in Fig. 3B. The practicality of the quantitative method was verified by designing accuracy, precision, linearity, limit of detection (LOD) and limit of quantitation (LOQ) experiments [19]. A standard curve was established to describe the linearity of peak area (y) versus control concentration (x), and the correlation coefficients of the three curves showed good linearity ($r \geq 0.99$) in the concentration range. LOD and LOQ were shown in Table S1. The accuracy was expressed by the recovery experiment. The mean recovery of the standard spiking method was 96.3%, 96.3% and 103.9% (RSD < 2%), respectively. The results show that the method is accurate and reliable for the determination of the three compounds in AM.

4.1.2 Quantification of three components in AM

In this study, the quantification of the three examined components within the samples was accomplished using the external standard method. The results of the component content analysis are graphically represented in Fig. 2A and Table S1. Evidently, the content levels of the three components across the 20 batches of AM samples exhibited substantial fluctuations. Notably, among these components, the content of IA is the lowest (0.06 μg/mL), whereas the content of Bai is the highest (0.34 μg/mL).

4.1.3 Five-wavelength fusion fingerprint analysis (FWFFP)

The composition of TCM is complex, and a single wavelength can't adequately reflect the properties of the contained substances. Therefore, we used a multi-wavelength fusion method to comprehensively evaluate the various substances in the samples. The main chemical components of AM, CA (peak 6), IA (peak 13) and Bai (peak 16), have strong UV absorption at 220 nm, 238 nm, 254 nm, 278 nm and 326 nm, respectively. In addition, the UV absorption of the samples at different wavelengths differed significantly. Therefore, to highlight the UV absorption characteristics of each substance, a five-wavelength maximum fusion

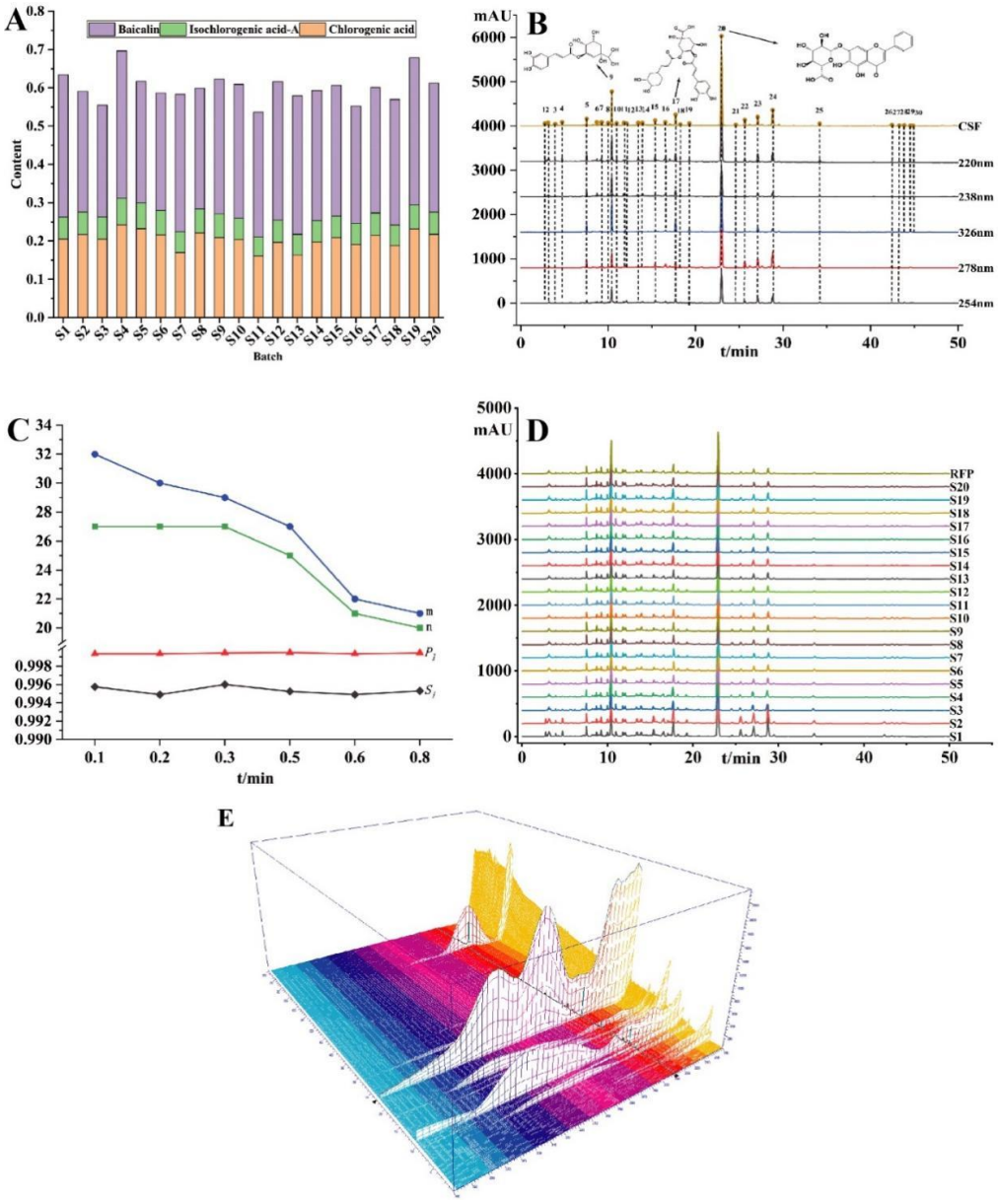

Fig. 3 Content (μg/mL) of three quantitative components in each batch (A), FWFFP and three quantitative component structures (B), changes in various parameters under different fusion windows (C), FWFFP of 20 batches of AM (D) and 3D plot of AM (E)

fingerprint was used to combine the maximum UV absorption characteristics of the five chromatograms within a new fusion chromatogram (CSF) [20]. The number of common fingerprint peaks at different wavelength was 22 (220 nm), 22 (238 nm), 22 (254 nm), 18 (278 nm) and 12 (326 nm), as shown in Fig. 3B.

There is an important parameter in FWFFP, the fusion window. The numerical size of the fusion window affects the number of peaks in the CSF, and the larger the fusion window, the fewer the CSF peaks. Therefore, it is necessary to select the appropriate fusion windows. The fusion window was selected mainly based on the number of peaks and

peak separation after fusion, where the more peaks, the better and the peaks with separation less than 1.5 are the better [14]. Fig. 3C shows the fusion window under different parameters, among which m means peak number and n means peak with separation more than 1.5. The fusion window determined by the above conditions is 0.2 min. The chromatographic signals of 20 batches of samples were input into the software in section 3.4. The fusion was performed by selecting the maximum peak pattern with a fusion window of 0.2 min, and a five-wavelength fusion fingerprint with 30 shared peaks was generated. The fusion fingerprints generated from different batchs were merged into one image, as shown in Fig. 3D.

4.1.4 Clustering using a Gaussian Mixture Model

Gaussian Mixture Model (GMM) is an unsupervised machine learning method for clustering ungrouped data [21], which can be adapted to different data complexities and structures by adjusting the number of components. The maximum expectation algorithm is used in half of the algorithm estimation process of GMM. In this study, the samples were clustered and analyzed by using the GMM model with parameters estimated by the maximum expectation algorithm. The peak area of 30 fused fingerprint peaks of 20 batches of samples were used as parameters, the data format was organized and extracted by python, and clustering was performed by the established model. As the 3D plot in Fig. S1A shows, the first three principal components of this result explained 64.53% of the data. All the samples were classified into three groups from the 2D projection diagrams (Fig. S1B), in which 8,10 and 11 constituted the first group, 2, 3, 5, 6, 15 and 16 the second, and the rest the third. The second group is mostly negatively correlated with PC3. S4 and s7 in the third group are positively correlated with PC1, PC2 and PC3, while s14 are strongly negatively correlated. The farther the peaks are from the origin, the greater the contribution. The results show that the model initially distinguishes the fluctuation of different substances and the variability of the samples, but the variability of the samples and the overall quality consistency caused by the differences in the content of each component need to be evaluated in a more comprehensive and scientific way.

4.1.5 Evaluating FWFF by CLQFM

The fusion fingerprints were evaluated using the software mentioned in section 3.4, and the results are shown in Table 1. The spectra at different wavelengths were fused as shown in Fig. 3B and imported into the evaluation software, and the overall RFP of the samples was obtained by averaging the fused spectra of all the samples and evaluating the grade of the samples by CLQFM. $\boldsymbol{S}_{\mathrm{L}}$ ranged from 0.990 to 0.998, indicating that the substances in different batches of samples are similar and the chemical fingerprints are evenly distributed. $\boldsymbol{P}_{\mathrm{L}}$ ranged from 88.5% to 114.7%, suggesting that the chemical content of the samples varied. Table S3 shows the evaluation results of five single wavelengths. The fused fingerprints differ from the evaluation results of single wavelengths, indicating that single wavelengths may have latent information, which can be identified by fused fingerprints. At the same time, although the sample composition was complex, the differences between batches were not significant; therefore, the properties of the contained substances could not be completely reflected by using HPLC alone, and the evaluation needed to be combined with other analytical methods.

Table 1 S_L, P_L, and grade of 20 batches of AM with HPLC, UV-QFP, UVSD, Fusion-CSF, HPLC+UV, and ECFP, with *E* values

No.	HPLC-238 nm			UV-QFP			UVSD			FWFFP			ECFP			Integrated			*E*
	S_L	P_L%	Grade	S_L	P_L%	Grade	S_L	P_L%	Grade	S_L	P_L%	Grade	S_{EC}	P_{EC}%	Grade	S_L'	P_L'%	Grade	
S1	0.997	106.6	2	0.999	66.2	6	0.948	58.6	7	0.995	109.1	2	0.951	106.3	2	0.982	87.2	3	0.214
S2	0.996	96.0	1	1.000	100.5	1	0.990	103.2	1	0.997	95.2	1	0.975	108.1	2	0.991	98.0	1	0.194
S3	0.994	89.9	3	1.000	84.9	4	0.981	80.0	5	0.996	88.5	3	0.974	96.7	3	0.99	86.9	3	0.179
S4	0.998	114.7	3	1.000	119.7	4	0.996	125.4	5	0.998	114.7	3	0.914	124.1	7	0.971	117.2	4	0.183
S5	0.991	98.6	1	1.000	108.5	2	0.995	106.9	2	0.990	96.3	1	0.992	112.4	4	0.994	102.8	1	0.156
S6	0.991	94.7	2	0.999	85.8	3	0.981	81.2	5	0.991	92.8	2	0.986	103.8	3	0.992	89.6	3	0.147
S7	0.994	100.5	1	1.000	66.0	6	0.964	62.0	6	0.997	104.8	1	0.997	101.5	2	0.998	84.7	4	0.160
S8	0.995	96.8	1	0.999	247.1	8	0.894	221.4	8	0.995	95.6	1	0.992	111.7	4	0.995	171.6	8	0.153
S9	0.997	103.5	1	1.000	77.4	5	0.974	73.4	5	0.997	104.7	1	0.971	92.6	2	0.989	90.9	2	0.041
S10	0.998	101.7	1	1.000	190.0	8	0.951	204.6	8	0.998	100.2	1	0.969	88.3	3	0.989	145.4	7	0.146
S11	0.994	92.1	2	1.000	90.7	2	0.987	89.2	4	0.996	94.3	2	0.478	355.9	8	0.825	92.1	2	0.154
S12	0.998	103.7	2	1.000	84.2	4	0.979	82.4	4	0.997	106.2	2	0.984	92.3	4	0.994	94.8	2	0.174
S13	0.99	99.5	2	0.999	68.3	6	0.957	63.3	6	0.994	105.1	2	0.997	89.2	3	0.997	85.8	3	0.141
S14	0.993	99.1	1	0.999	62.7	6	0.948	54.7	7	0.993	98.7	1	0.993	89.8	3	0.995	80.8	4	0.155
S15	0.996	100.8	1	1.000	62.7	6	0.952	55.7	7	0.996	99.8	1	0.968	100.3	2	0.988	81.4	4	0.159
S16	0.998	91.5	3	1.000	103.5	1	0.993	102.7	3	0.997	89.1	3	0.994	86.1	4	0.997	96.7	1	0.153
S17	0.998	98.3	1	1.000	187.8	8	0.959	199.8	8	0.998	96.3	1	0.952	95.1	2	0.983	142.4	7	0.165
S18	0.997	95.9	1	1.000	62.0	6	0.954	55.6	7	0.997	95.7	1	0.990	89.8	3	0.996	78.9	5	0.179
S19	0.998	112.2	3	1.000	67.2	6	0.954	61.2	6	0.997	111.2	3	0.926	114.5	4	0.974	89.4	3	0.161
S20	0.998	100.9	1	1.000	64.4	6	0.947	57.7	7	0.998	100.7	1	0.840	140.1	6	0.946	82.6	4	0.157

Para	1	2	3	4	5	6	7	
S_L	≥0.95	≥0.90	≥0.85	≥0.80	≥0.70	≥0.60	≥0.50	< 0.50
P_L%	95-105	90-110	85-115	80-120	70-130	60-140	50- 150	< 50 or >150
α	≤0.05	0.05-0.10	0.10-0.15	0.15- 0.20	0.20-0.30	0.30-0.40	0.40--0.50	> 0.50

4.2 UV spectrum fingerprint analysis

4.2.1 Methodology validation

The precision was determined by repeating the injection six times, the reproducibility was determined by preparing six samples in parallel, and the sample stability was determined by analyzing S13 at room temperature after 0, 2, 4, 6, 8 and 12 h. The RSD values of the peak areas of each quantum peak were less than 3.7%, 1.1% and 3.4%, respectively. The results showed that the method can be used to analyze UV spectra.

4.2.2 Second-order derivative of the UV spectrum (UVSD)

Second-order derivative spectroscopy is a method of wave spectral analysis defined as a new curve obtained by applying second-order derivatives to a spectral curve, and is often used to find features such as peaks, valleys and inflection points in a spectrum. The method is based on the property that the second-order derivative is zero at the extreme points of the function and alternately positive and negative at the inflection points of the function. By performing second-order derivative operations on the spectrum, features such as peaks, troughs and inflection points in the spectrum can be significantly improved, making them easier to analyze and identify.

The UV data underwent second-order processing and were subsequently saved in *.csv format files, as shown in Fig. 4A. These files were then imported into the software described in section 3.4 for thorough analysis, the outcomes of which are shown in Table 1.

Notably, the results derived from the UV analysis exhibited notable discrepancies when compared to the liquid phase results. This disparity primarily arises from the distinctive evaluation methodologies employed: the HPLC assessed each individual substance within the sample, whereas the UV analysis gauged the cumulative absorption of all substances present. Specifically, within the cohort of 20 sample batches, batches S8, S10 and S17 were categorized as inferior, displaying a discernible deviation from the remaining batches in the spectral curve. This outcome is consistent with the comprehensive evaluation results. Within the UV second derivative evaluation, noteworthy extreme values were observed across the four UV signals, specifically at wavelengths of 191 nm, 212 nm, 265 nm and 310 nm. These peaks are likely attributed to the manifestation of π-π* and n-π* transitions. The distinctive occurrence of extreme values among the different batches underscores minor content variations between the batches. This subtle discrepancy indicates a nuanced divergence in substance content across the various batches.

4.2.3 Establishment of UV quantitative fingerprinting (UV-QFP)

UV-QFP was established by UV spectra which contains a large amount of spectral information. Although each point can be used to evaluate the quality of the samples, the computation is large and complicated. Therefore, UV-QFP was used to process samples to obtain a more convenient way of processing the data. The data in CSV format obtained from 20 batches of samples were imported into the software described in Section 3.4, and the spectral quantitative fingerprint peaks were obtained according to Equations (8)-(10), and the spectral quantitative fingerprint profiles were obtained by optimizing the number of merged points. The original UV spectra (Fig. 4B) and the quantitative spectra (Fig. 4C) with different merging points (Fig. 4D) were processed separately using CLQFM, and the results obtained from different merging points were tested separately with the results obtained from

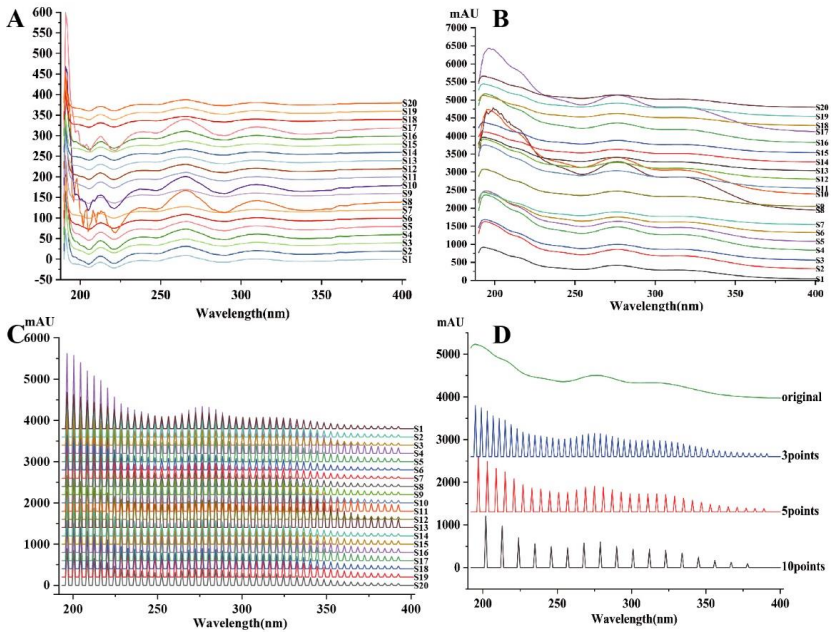

Fig. 4 Original UV spectrum (A), quantized ultraviolet spectroscopy (B), different merging points and original UV spectrograms (C), UV second-order derivative spectroscopy (D)

the original samples by *T*-test. The results showed that there was no significant difference between the evaluation results of different merging points, which indicated that the characteristic information of UV spectra was not changed. Finally, on the premise of retaining more information, three merging points were selected for data processing. According to Table 1, the $\boldsymbol{S}_{\text{L -UVFP}}$ of UV samples were all relatively close, but the $\boldsymbol{P}_{\text{L -UVFP}}$ had a large batch-to-batch difference, which indicated that the types of substances contained in different batches were more similar, but the contents differed greatly. Compared with the HPLC mapping, the grades of the same batches were significantly different, which indicated the potential applicability of UV mapping in the analysis of TCM. Therefore, spectral quantum fingerprinting can be used as a data processing method to analyze complex samples and reflect information that cannot be analyzed by HPLC.

$$H = Ab_{max} \tag{8}$$

(Ab_{max} denoted the maximum absorbance of the selected continuous wavenumber section).

$$A = \sum_{i=1}^{n} Ab_i \tag{9}$$

(A was the peak area of the quantum peak, and Ab_{i} was the derivative of absorbance for each wavenumber).

$$W_{\frac{1}{2}} = \frac{i}{200} \tag{10}$$

4.3 Electrochemical fingerprint analysis

4.3.1 Optimization of experimental conditions and Methodology validation

The experimental conditions were screened by performing orthogonal experiments, the solution concentration of the system for the BZ oscillation reaction was determined by screening a series of concentrations of sulfuric acid, malonic acid, ceric ammonium sulfate and potassium bromide, and the injection volume was determined by screening a series of linear volumes of samples, as shown in

Table S4 and Table S5. It is worth noting that when different volumes of samples are added, the larger the volume, the shorter the oscillation lifetime. This is due to the inhibition of the reaction or the acceleration of the reaction rate. The relationship between the volume and the oscillation lifetime can be expressed by a linear equation: y = -61637x + 5742.1, (r = 0.9967). The finalized experimental conditions are 2.0 mol/L sulfuric acid solution (H_2SO_4), 0.3 mol/L propane diacid solution ($CH_2(COOH)_2$), a 0.04 mol/L ceric ammonium sulfate solution (prepared using a 0.2 mol/L H_2SO_4 solution) and 0.3 mol/L potassium bromate ($KBrO_3$), and the sample volume is 0.05 mL.

The reproducibility was verified by measuring the samples (S11) five times consecutively. Good reproducibility was determined by calculating the relative standard deviations (RSD%) for each parameter. The RSD of the induction time (t_{ind}), the peak top time (t_{pt}), the peak potential (E_{pt}), the start of oscillation potential (E_{os}), the end of oscillation time (t_{oe}), the end of oscillation potential (E_{oe}), the oscillation lifetime (t_{ol}) and the maximum amplitude (ΔE_{max}) was 2.50%, 7.27%, 0.25%, 0.83%, 0.93%, 0.29%, 0.91% and 3.30%, respectively. The average RSD was 2.04%, indicating that the established method has good reproducibility and can be used for the determination of samples.

4.3.2 Analysis of ECFP

The eight characteristic parameters of ECFP were obtained by recording each time and potential in the electrochemical companion workstation software, among which t_{ind} and t_{pt} had the minimum and maximum RSD, respectively, indicating that they had the minimum and maximum fluctuations between different batches of samples. The electrochemical workstation displays the time as four valid digits and the potential as four decimal places, and the data obtained are shown in Table 2.

Table 2 Characteristic parameters of ECFP for all samples

No.	t_{ind}/s	t_{pt}/s	E_{pt}/V	E_{os}/V	t_{oe}/s	E_{oe}/V	t_{ol}/s	ΔE_{max}/V
S1	84.30	29.930	1.0178	0.8877	2203	0.8354	2118.7	0.1360
S2	89.05	16.200	1.0556	0.9157	2354	0.8537	2264.95	0.1248
S3	88.45	7.748	1.0772	0.9354	2971	0.8433	2882.55	0.1188
S4	91.05	8.050	1.0848	0.9400	2460	0.8706	2368.95	0.1155
S5	90.40	7.701	1.0888	0.9506	2648	0.8735	2557.6	0.1116
S6	92.10	6.150	1.0940	0.9580	2483	0.8851	2390.9	0.1050
S7	88.61	7.452	1.0955	0.9633	2569	0.8905	2480.39	0.1034
S8	82.75	6.849	1.0975	0.9687	2627	0.8822	2544.25	0.1047
S9	88.20	7.596	1.0816	0.9490	2440	0.8797	2351.8	0.1041
S10	87.90	7.201	1.0824	0.9571	2487	0.8833	2399.1	0.0998
S11	85.35	7.498	1.0814	0.9578	2791	0.8682	2705.65	0.1030
S12	85.50	7.502	1.0905	0.9698	2520	0.8928	2434.5	0.1022
S13	88.20	7.899	1.0891	0.9802	2296	0.9186	2207.8	0.1994
S14	90.90	6.851	1.0931	0.9796	2545	0.9013	2454.1	0.0925

(to be continued)

Continued table 2

S15	86.70	6.800	1.0946	0.9898	2545	0.9041	2458.3	0.0892
S16	88.20	7.899	1.0891	0.9802	2296	0.9186	2207.8	0.0872
S17	84.65	32.35	1.0007	0.8704	2717	0.7931	2632.35	0.1275
S18	87.39	8.098	1.0871	0.9724	2467	0.9026	2379.61	0.0995
S19	87.79	7.541	1.0918	0.9694	2550	0.8968	2462.21	0.0931
S20	83.85	7.299	1.0972	0.9846	2586	0.8970	2502.15	0.0971
Mean	87.57	10.23	1.0795	0.9540	2528	0.8795	2440.18	0.1107
Max	92.10	32.35	1.0975	0.9898	2971	0.9186	2882.55	0.1994
Min	82.75	6.150	1.0007	0.8704	2203	0.7931	2118.70	0.0872
RSD%	2.91	72.72	2.40	3.30	7.00	3.43	7.26	22.18

Since the sample addition was in a good linear relationship with the oscillation lifetime, the total amount of chemicals in the samples that inhibited the B-Z oscillations could be reflected indirectly, and the results showed that the order of the total compounds in the samples was:

S1>S16>S2>S9>S4>S18>S6>S10>S12>S14>S15>S19>S7>S20>S8>S5>S17>S11>S3>S13.

Combined with Fig. 2B, it can be seen that the Potential-Time (*E-T*) curves of different batches of AM are more similar, but there are some differences in the oscillation lifetime, which indicates that different batches of AM have different inhibition degrees on the oscillation reaction, while having similar chemical compositions. Among them, S3, S11, and S17 had fewer chemical compositions or lower compositional activities than other batches but showed longer oscillatory lifetime, while S1 showed the strongest inhibition and had the shortest oscillatory lifetime. In conclusion, longer oscillation lifetime represents more active components under the same spiking volume conditions.

Meanwhile, the electrochemical samples were analyzed by Hierarchical Cluster Analysis (HCA), and the eight characteristic parameters were imported into SIMCA software. The clustering results are shown in Fig. S2. Compared with the results in section 4.1.4, the HCA results showed significant differences. This is because GMM clustering uses fused peak areas, which represent the content of each component, whereas the electrochemical parameters represent the overall ability of the substance to inhibit the B-Z oscillation reaction as well as the strength of its involvement in the redox reaction.

4.3.3 Evaluating ECFP by CLQFM

The *.csv file exported from the companion software for the electrochemical workstation was imported into the software mentioned in 3.4 and the RFP of ECFP was generated for the 20 batches of samples. CLQFM was used to evaluate the ECFP, and the mean method was used to generate the RFP of the ECFP, followed by the evaluation of the 20 batches of AM. Since the addition of the sample in electrochemistry inhibited the reaction, $\boldsymbol{P}_{EC}$ was used to express the content of the sample as shown in Eq. (11). $\boldsymbol{P}_{EC}$ is negatively correlated with $\boldsymbol{P}_{L}$, indicating that the less the active ingredient in the sample, the greater the $\boldsymbol{P}_{EC}$, and the evaluation results are shown in Table 1. Among them, $\boldsymbol{S}_{L} > 0.8$ represents the similarity of chemical composition between samples, and all the samples are above 0.84, indicating that there is little difference in

composition between batches of samples. $\boldsymbol{P}_{\mathrm{L}}$ represents the content of substances contained in the samples, and the corresponding $\boldsymbol{P}_{\mathrm{EC}}$ fluctuates between 86.1 and 355.9, which indicates that the content of components varies a lot between batches of samples. S16 is the smallest and S11 is the largest, indicating that the degree of inhibition on the system is greatest for S16 and smallest for S11. This result is different from the results obtained by using the eight characteristic parameters, mainly because the parameters only consider a particular condition, while the evaluation using CLQFM considers the overall characteristics of the samples, and is more comprehensive and objective. Therefore, using the CLQFM method for evaluation in ECFP is a better approach.

$$\boldsymbol{P}_{\mathrm{EC}} = 1/\boldsymbol{P}_{\mathrm{L}} \quad (11)$$

4.4 Online in vitro antioxidant activity assay

The three main components in TCM have some antioxidant capacity [22,23], so it is meaningful to measure their antioxidant capacity. DPPH is dark in color and high in absorbance. After oxidation, the color becomes ligher, and the absorbance decreases, showing an inverted peak in the chromatogram. The flow rate was optimized according to the shape and size of the inverted peak signal. The finalized measurement conditions were a 5-fold dilution and a flow rate of A 0.4 mL/min, B 0.3 mL/min. In this study, the *E*-value was used to evaluate the antioxidant capacity of the samples. The larger the *E*, the stronger the antioxidant capacity.

The antioxidant activity of 20 batches of samples was determined using on-line *in vitro* antioxidant assay and the results are shown in Table 1. All the samples showed antioxidant activity and the RSD of *E* value was 20.75%, indicating that the samples are different in antioxidant activity. The largest *E* was 0.214 for S1 and the smallest was 0.041 for S9, ranking 2 and 1 respectively, and indicating that the potential antioxidant capacity for analysis. The gray correlation of the three substances were CA 0.79, IA 0.81 and Bai 0.83. Among all the peaks, Bai has the highest correlation, indicating that Bai is the main provider of antioxidant capacity in the samples. The content of IA is the lowest among the three, but it reflects a certain antioxidant capacity, indicating that the substance had a strong antioxidant capacity. In contrast, the antioxidanct capacity of CA is weak.

4.5 Relationship of HPLC, UV and ECFP between antioxidant activity

As shown in Table 1, the *E* values of 20 batches of samples ranged from 0.041-0.214, indicating that all samples had strong antioxidant activity. Meanwhile, the *E* value fluctuated very little, indicating that the chemical compositions of the samples were similar and the active content differences were small. In order to further explore the relationship between antioxidant activity and fingerprinting components, the peak areas of 30 common characteristic peaks of 20 batches of TCM and their *E* values were subjected to gray correlation analysis. In the gray correlation analysis, if the correlation coefficient was greater than 0.8, the factor was considered to have high correlation with the dependent variable. The 30 shared peaks of fusion fingerprint were subjected to gray correlation analysis with *E* to obtain the correlation between each shared peak and *E*, as shown in Fig. 5B. Among them, 12 peaks were greater than 0.8, among which peak 17 is IA, and peak 20 is Bai, indicating that two of the three substances have strong antioxidant activity. Meanwhile, there are unidentified three peaks, namely 2, 4 and 8, whose large correlation coefficients suggested antioxidant activity. The 50 quantum peaks in the quantified UV spectrum were analyzed separately with *E* by gray correlation, and the results are shown in Fig. 5C. No

peak had a correlation coefficient greater than 0.8, but all of them were around 0.72, and the correlation coefficients of the peaks were relatively close. It does not necessarily mean that the antioxidant activity of the substance corresponding to a specific segment of UV absorption wavelength is better, but that the substance as a whole provides antioxidant activity. At the same time, a bump was shown around 210 nm as well as around 290 nm, indicating that the antioxidant capacity of the substance exhibiting higher absorbance at this location is relatively high. The data processing model provides a rapid, wide-area screening method for substances with antioxidant capacity.

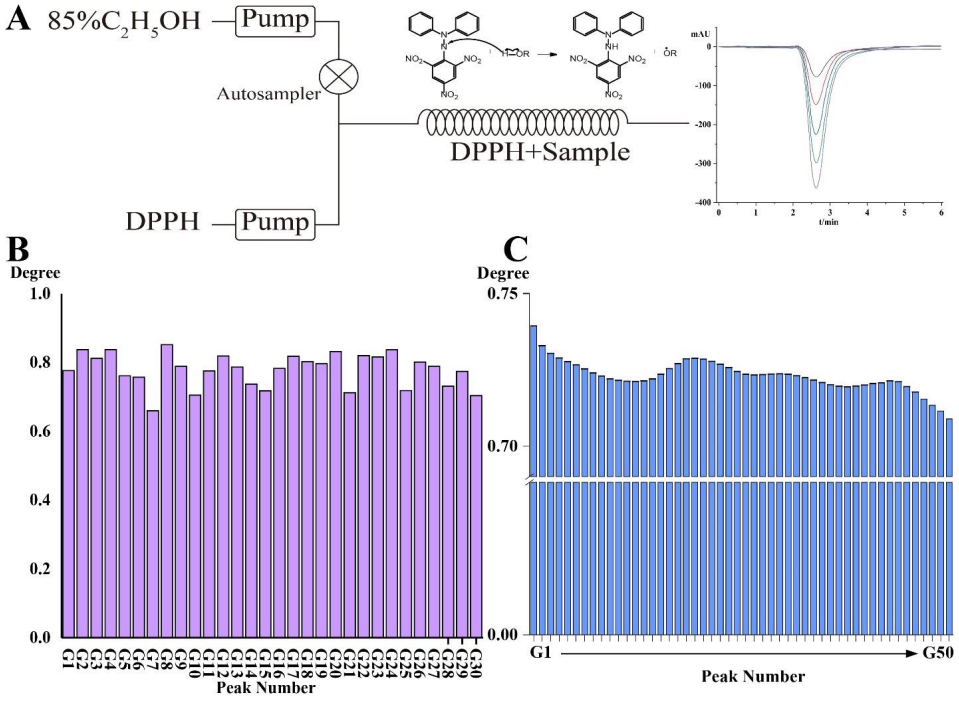

Fig. 5 Online *in vitro* antioxidant activity measurement system scheme (A), grey correlation degree of all peaks and *E* values in FWFFP (B), grey correlation degree of all quantum peaks and *E* values in UV-QFP (C)

With regard to ECFP, the grey correlation coefficients of each parameter related to the *E* value are shown in Fig. 2C, the grey correlation coefficients of all the parameters are greater than 0.8, indicating that there is an obvious correlation between the electrochemical parameters and antioxidant capacity, which is precisely because the B-Z oscillation reaction is a redox reaction, and the addition of the sample inhibited the reaction, indicating the sample has a certain redox capacity, thus exhibiting this highly correlated relationship.

4.6 Equally weighted fusion fingerprinting of HPLC, UV and ECFP

The evaluation results of HPLC and UV fingerprints reflect the compositional content and structural differences of AM, respectively. Where the HPLC results reflected the independent substances in the sample, the UV and ECFP reflected the overall substance composition of the sample. In order to achieve a comprehensive evaluation of TCM, as shown in Equations (12) and 5 Conclusion, these

three different methods were integrated by equal weight fusion, and a new sample quality level was obtained. As Table 1 shows, integrated evaluation results are not the same compared to HPLC, UV and ECFP. The grades of 11 batches of samples in integrated evaluation and in three methods are completely different. For example, S7 obtained grade 1 in HPLC, grade 6 in UV-QFP, grade 2 in ECFP, and grade 4 in comprehensive evaluation. $\boldsymbol{S}_{\mathrm{L}}$' of all the samples ranged from 0.825 to 0.998, indicating that the chemical composition of the samples is extremely similar. $\boldsymbol{P}_{\mathrm{L}}$' ranged from 78.9 to 171.6, indicating that the content of the substances in the samples varies. $\boldsymbol{S}_{\mathrm{L}}$' and $\boldsymbol{P}_{\mathrm{L}}$' values are different when comparing the results of HPLC, UV and ECFP, because these three methods have their own one-sidedness, If one method alone does not adequately reflect the quality of the sample, it is necessary to carry out a comprehensive evaluation.

$$S_{\mathrm{L}}' = \frac{1}{3}(S_{\mathrm{L-HPLC}} + S_{\mathrm{L-UV}} + S_{\mathrm{EC}}) \quad (12)$$

$$P_{\mathrm{L}}' = \frac{1}{3}(P_{\mathrm{L-HPLC}} + P_{\mathrm{L-UV}} + P_{\mathrm{EC}}) \quad (13)$$

5 Conclusion

This research aims to achieve the comprehensiveness and effectiveness of quality control by employing a combination of quantitative and qualitative analyses, bolstered by integrated techniques like HPLC, electrochemical and UV-QFP. The utilization of HPLC allowed for precise quantification, UV-QFP provided qualitative insights, and ECFP showed the redox activities of the samples. By merging the outcomes of these three techniques, a comprehensive evaluation of the samples was achieved. Notably, the UV signals were transformed into a chromatogram featuring 50 distinct peaks by quantum fingerprint, thereby realizing quantitative fingerprinting analysis. To assess similarity between samples and control formulations, the CLQFM was employed, using parameters such as $\boldsymbol{S}_{\mathrm{L}}$, and $\boldsymbol{P}_{\mathrm{L}}$. Meanwhile, the combination of electrochemistry and drug analysis through the introduction of $\boldsymbol{P}_{\mathrm{EC}}$ provided new ideas for drug analysis. Additionally, the antioxidant capacity of the samples was measured to further enrich the quality evaluation scope of these formulations. Incorporating a holistic approach, this study also introduced a gray correlation model. This model effectively revealed the relationship between HPLC results, UVFP data, ECFP results and antioxidant capacity measurements. By amalgamating these diverse aspects, a robust and practical framework for evaluating in-hospital formulations was established. This method not only improves the accuracy and thoroughness but also provides a versatile method for the quality consistency control of hospital preparations.

Conflict of interest

No potential conflict of interest was reported by the authors.

Acknowledgment

This study was supported by the National Natural Science Foundation of China (No. 81573586).

References

[1] Zhang JH, Wider B, Shang HC, et al. Quality of herbal medicines: Challenges and solutions. Complement Ther Med, 2012, 20: 100-106.

[2] Yang LP, Xie XM, Yang L, et al. Monitoring quality consistency of Ixeris sonchifolia (Bunge) Hance injection by integrating UV spectroscopic fingerprints, a multi-wavelength fusion fingerprint method, antioxidant activities and UHPLC/Q-TOF-MS. RSC Adv, 2016, 6:

87616-87627.

[3] Xu CL, Shi Y, Xu H, et al. Comparative investigation between raw and stir-frying processed Cuscutae Semen based on HPLC fingerprints coupled with chemometric methods. J Aoac Int, 2023, 4: 1037-1047.

[4] Gu W, Sun M, Yang WT, et al. Effects of TCMs and Lactobacillus strains on immunosuppressed mice and bacteriostatic effect on Escherichia coli K88 after fermentation, Biotechnol Biotec EQt, 2019, 33: 1291-1302.

[5] Chen JC, Wu HL, Wang T, et al. High-Performance Liquid Chromatography-Diode Array Detection Combined with Chemometrics for Simultaneous Quantitative Analysis of Five Active Constituents in a Chinese Medicine Formula Wen-Qing-Yin. Chemosensors, 2022, 10: 238.

[6] Wu L, Ni ZH, Xu YC, et al. Investigation on the Characteristic Components of Dahuang Zhechong Pill Based on High-Performance Liquid Chromatography (HPLC) Fingerprint. Nat Prod Commun, 2019, 14: 1-8.

[7] Wang PY, Wang XY, Li YF, et al. Thorough evaluation of the Chinese medicine preparations and intermediates using high performance liquid chromatography fingerprints and ultraviolet quantum fingerprints along with antioxidant activity: Shuanghuanglian oral solution as an example. J Chromatogr A, 2023, 1705: 464196.

[8] Yang FL, Chu TT, Zhang YJ, et al. Quality assessment of licorice (Glycyrrhiza glabra L.) from different sources by multiple fingerprint profiles combined with quantitative analysis, antioxidant activity and chemometric methods. Food Chem, 2020, 324: 126854.

[9] Jaccoulet, E, Boughanem C, Auduteau L, et al. UV spectroscopy and least square matching for high throughput discrimination of taxanes in commercial formulations and compounded bags. Eur J Pharm Sci, 2018, 123: 143-152.

[10] Li X, Zhang F, Wang X, et al. Evaluating the quality consistency of Rong'e Yishen oral liquid by UV + FTIR quantum profilings and HPLC fingerprints combined with 3-dimensional antioxidant profiles. Microchem J, 2021, 170: 106715.

[11] Sun GX, Yang T, Sun WY, et al. Key technology of TCM consistency evaluation—— Theory and application of spectral quantum fingerprints in quality consistency evaluation of TCM. Central South Pharmacy, 2022, 20: 1467-1477.

[12] Wang XY, Chang Q, Lan, et al. Reliability evaluation of traditional Chinese medicine fingerprints combined with qualitative and quantitative analysis and antioxidant activity to comprehensively evaluate the quality of Citri Reticulatae Pericarpium. New J Chem, 2022, 46: 21660-21671.

[13] Gong DD, Chen JY, Li X, et al. A smart spectral analysis strategy-based UV and FT-IR spectroscopy fingerprint: Application to quality evaluation of compound liquorice tablets. J Pharmaceut Biomed, 2021, 202: 114172.

[14] Yang HZ, Yang T, Gong DD, et al. A trinity fingerprint evaluation system of traditional Chinese medicine. J Chromatogr A, 2022, 1673: 1037-1047.

[15] Jia GC, Wang HX, Ye RP, et al. Application progress on electrochemical oscillation fingerprint in quality control of Chinese materia medica. Chinese Traditional Herb, 2019, 50: 5064-5070.

[16] Dou XW, Yang LP, Liu ZB, et al. Evaluation of Renshen Guipi Wan quality by linearly quantified fingerprint method based on three-wavelength high performance liquid chromatographic fingerprints. Chin J Chrom, 2013, 31: 456.

[17] Zhang Y, Lan LL, Gong DD. Evaluation of Fusion Fingerprint for Tuire Jiedu Injection by Comprehensive Linear Quantitative Fingerprint Method. Journal of Instrumental Analysis, 2021, 40: 79-85.

[18] Gyorgyi L, Turanyi T, Field RJ. Mechanistic details of the oscillatory Belousov-Zhabotinskii reaction. J Phys Chem, 1990, 94: 7162-7170.

[19] Masumeh Z, Morteza E, Reza M, et al. Spectrophotometric analysis of thrombolytic activity: SATA assay. BioImpacts: BI, 2018, 8: 31-38.

(to page 151)

Acknowledgements

We would like to show our great appreciation to Shenyang Zhuoyuehefa Pharmaceutical Co. and Grand Life Science (Liaoning) Co., LTD. for their financial support on this scientific expedition and Shenyang Pharmaceutical University for their great support and help to the 10th Scientific Research Team on Chinese Medicine Resources.

References

[1] Zhang L. The Fanjing Mountains in the Wuling Mountains. Western China, 2005, 2: 9.

[2] Ma Y. Ecotourism resources and development in Fanjing Mountain area of northeast Guizhou. J Anhui Agric Sci, 2007, 32: 10413-10415.

[3] Zhu JY. Global comparative analysis of plant diversity and world heritage value of Fanjing Mountain. Guizhou Normal University, 2017.

[4] Huang CQ. Ecological environment and tourism development of Fanjing Mountain. Tourism Overview (the second half of the month), 2016, 04: 223-225.

[5] Editorial Committee of the Flora of China, Chinese Academy of Sciences. Flora of China. Beijing: Science Press, 2007.

[6] Chen QH. Flora of Guizhou. Guizhou Science and Technology Press, 2004.

[7] Editorial Committee of Chinese Materia Medica, State Administration of Traditional Chinese Medicine. Chinese Materia Medica. Shanghai: Shanghai Science and Technology Press, 1999.

[8] National Compilation of Chinese Herbal Medicines. Beijing: People's Health Publishing House, 1976.

(from page 136)

[20] Chang Q, Lan LL, Gong DD, et al. Evaluation of quality consistency of herbal preparations using five-wavelength fusion HPLC fingerprint combined with ATR-FT-IR spectral quantized fingerprint: Belamcandae rhizoma antiviral injection as an example. J Pharmaceut Biomed, 2022, 214: 114733.

[21] Saranya S, Poonguzhali S, Karunakaran S. Gaussian mixture model based clustering of Manual muscle testing grades using surface Electromyogram signals. Phys Eng Sci Med, 2020, 43: 837-847.

[22] Paudel KR, Kim DW. Microparticles-Mediated Vascular Inflammation and its Amelioration by Antioxidant Activity of Baicalin. Antioxidants, 2020, 9: 890.

[23] Corrigan H, Dunne A, Purcell N, et al. Conceptual functional-by-design optimisation of the antioxidant capacity of trans-resveratrol, quercetin, and chlorogenic acid: Application in a functional tea. Food Chem, 2023, 428: 136764.